Supplement of Hydrol. Earth Syst. Sci., 30, 5711–5734, 2026
https://doi.org/10.5194/hess-30-5711-2026-supplement
© Author(s) 2026. CC BY 4.0 License.

Hydrology and Earth System Sciences
Open Access

Supplement of

Effects of spatial soil moisture variability in forest plots on model parametrization and simulated groundwater recharge estimates

Thomas Fichtner et al.

Correspondence to: Thomas Fichtner (thomas.fichtner@tu-dresden.de)

The copyright of individual parts of the supplement might differ from the article licence.

Model description

The following section outlines the conceptual representation of water fluxes and storage dynamics implemented in the model, describing the main hydrological processes along the soil–vegetation–atmosphere continuum and draws on the detailed process descriptions provided by (Bernhard et al., 2020; Federer et al., 2003).

Model structure

Precipitation (water or snow) first interacts with the canopy, where it is either intercepted and subsequently evaporated or transmitted to the soil surface as throughfall. Water reaching the ground may infiltrate, freeze, evaporate, generate surface runoff, percolate to deeper layers or be retained as soil moisture. Infiltrating water is partitioned between matrix flow and macropore bypass flow and distributed vertically through the soil profile using a top-down approach. Soil water dynamics are simulated based on numerical approximations of the Richards equation (Richards, 1931) using the Mualem–van Genuchten hydraulic parameterization (van Genuchten, 1980). The soil column includes components for groundwater recharge, seepage and lateral downslope flow. Soil water stored within the profile supplies evaporation from upper layers and root water uptake for transpiration.

Evapotranspiration processes

Evapotranspiration is calculated using a modification of the Penman–Monteith framework proposed by (Shuttleworth and Wallace, 1985), which allows the total latent heat flux to be partitioned into its individual components: evaporation of intercepted water (or snow), plant transpiration and evaporation from bare soil (or snow surface). The approach applies a "single big-leaf" representation of the canopy and conceptualizes the system as two coupled layers, canopy and soil, linked by aerodynamic and surface resistances.

Evaporation of intercepted water and snow

Interception storage is parameterized as a function of leaf area index (LAI) and stem area index (SAI), assuming a constant storage capacity per unit leaf and stem area. Partial canopy wetting and drying are not explicitly represented. As long as intercepted water or snow is present, evaporation to the atmosphere occurs at a rate determined primarily by atmospheric demand and aerodynamic resistance, assuming negligible stomatal resistance. Thus, evaporation of interception is energy- and vapor-pressure-gradient driven and can proceed at near-potential rates until canopy storage is depleted ((Brutsaert, 1982; Gash, 1979; Rutter et al., 1971).

Transpiration through stomata

Potential transpiration through stomata is calculated by solving for canopy latent heat flux under non-water-limited conditions. Canopy conductance is parameterized by a multiplicative approach, where maximum stomatal conductance (GLMAX) is reduced by stress functions dependent on incoming radiation (light limitation), air temperature and vapor pressure deficit (VPD). Aerodynamic resistances are determined by canopy height, LAI and wind speed, reflecting turbulent transport efficiency above and within the canopy.

Actual transpiration is computed as the minimum of potential transpiration and the hydraulically available soil water supply. The supply limitation is derived from a soil–plant hydraulic continuum that includes vertical root density distribution, soil water potential, rhizosphere resistance between bulk soil and root surface, root and xylem hydraulic resistances and critical leaf water potential. Under dry soil conditions, declining soil hydraulic conductivity increases rhizosphere resistance and restricts water flow to roots, thereby reducing transpiration even if atmospheric demand remains high.

Evaporation from soil

Throughfall and snowmelt, simulated by using a degree-day approach for estimating the snow energy balance (Rutter et al., 1971), reaching the soil surface, are subject to the potential soil evaporation, which is calculated separately from canopy transpiration, accounting for the available net radiation reaching the soil surface after attenuation by the canopy. The flux is controlled by aerodynamic resistance between soil surface and canopy air space as well as soil surface resistance. Soil surface resistance depends on soil water potential in the uppermost soil layer. As soil dries, capillary connectivity to the surface decreases and soil hydraulic conductivity declines sharply, increasing surface resistance and reducing evaporation. Thus, soil evaporation transitions from energy-limited to soil-moisture-limited conditions as drying progresses. When a snowpack is present, evaporation from the snow surface is computed based on aerodynamic resistance and the vapor pressure gradient between the snow surface and the atmosphere. Snowmelt is simulated using a degree-day approach, but sublimation and evaporation are physically linked to atmospheric demand.

Vegetation dynamics

Seasonal vegetation dynamics are incorporated via prescribed or phenology-based LAI development. LAI typically follows piecewise linear transitions between seasonal minimum and maximum values, driven either by fixed dates (e.g., budburst and leaf fall as well as leaf-area-index variations) or by temperature-based degree-day approaches.

Soil surface runoff

At the soil surface, water is partitioned into infiltration and rapid runoff pathways. Infiltration may occur as matrix flow into the uppermost soil layer or as preferential macropore bypass flow directly to deeper horizons. Under saturated conditions, a fraction of water can contribute immediately to stormflow via variable source areas or macropore flow combined with downslope drainage. Delayed runoff originates from soil drainage and from discharge of the groundwater store, which is represented as a linear reservoir releasing a fixed fraction of its storage per day, with optional deep seepage losses. Infiltration is conceptualized as instantaneous, without explicit surface ponding storage.

Soil water dynamics

Within the soil profile, which consists of multiple horizons with distinct hydraulic properties, vertical water movement is simulated using the Richards equation (Richards, 1931) for variably saturated flow. Fluxes are driven by gradients in total hydraulic potential and controlled by the soil hydraulic conductivity, parameterized with the Mualem–van Genuchten functions (van Genuchten, 1980; Mualem, 1976). This formulation requires horizon-specific parameters (θs, θr, α, n, Ks, τ) that define both the soil water retention curve and the unsaturated hydraulic conductivity function.

Soil water storage is described by the water retention relationship between volumetric water content (θ) and matric potential. For each soil layer, changes in storage result from the balance of incoming and outgoing fluxes (infiltration, percolation, root uptake, and evaporation). As soils dry, matric potentials decline and hydraulic conductivity decreases nonlinearly, strongly limiting vertical redistribution and reducing the availability of water for plant uptake. Conversely, near saturation, high conductivities facilitate rapid percolation and redistribution across layers. In this way, the retention and conductivity functions jointly control both the storage capacity of each horizon and the rate at which water can move through the profile.

Simultaneously, water is extracted from the soil by roots according to a vertically distributed root density profile. Root water uptake is governed by hydraulic resistances along the soil–plant–atmosphere continuum, including rhizosphere, root, and xylem resistances, and is constrained by a critical leaf water potential that regulates stomatal closure. Thus, soil water dynamics emerge from the coupled interaction of storage, vertical flow, and plant water uptake processes within the variably saturated soil column.

Subsurface drainage and conceptual groundwater dynamics

Water percolating from the deepest soil layer is transferred to a conceptual groundwater reservoir (vrfln), which represents recharge leaving the modeled soil profile. This flux is interpreted as deep drainage beyond the rooting zone and marks the lower boundary of the one-dimensional soil column. No explicit groundwater table dynamics are simulated; instead, recharge accumulates in a lumped linear storage.

Groundwater discharge is represented as a linear reservoir process, in which a constant fraction of the stored groundwater volume is released each day as baseflow. The proportionality factor defines the characteristic recession behavior and controls the temporal smoothing of recharge signals. In addition to baseflow generation, optional deep seepage losses can be specified to account for water that permanently leaves the modeled catchment system (e.g., regional groundwater flow).

Model limitations

Despite its physically based formulation, the model includes several structural simplifications that constrain its applicability and interpretation of results.

The model is strictly one-dimensional, resolving water fluxes only vertically at the point scale. Lateral subsurface flow and stormflow can be included conceptually, but no explicit spatial routing exists, limiting its use for distributed catchment-scale simulations.

Further, vegetation is represented as a single “big-leaf” canopy, neglecting vertical heterogeneity, multi-species interactions and partial canopy wetting/drying. Interception storage is fixed per unit leaf and stem area and within-canopy energy and radiation dynamics are simplified.

Infiltration is conceptualized as instantaneous, with no dynamic surface ponding. Macropore flow is represented via prescribed depth distributions rather than fully physical dual-permeability formulations, which may reduce accuracy in structured soils or during extreme rainfall.

Snow processes are simulated using a degree-day approach rather than a full energy balance, limiting accuracy where radiation, wind or humidity strongly affect accumulation and melt.

Plant water uptake assumes predominantly isohydric regulation, constrained by a critical leaf water potential. Root distribution and hydraulic properties are fixed and dynamic hydraulic traits such as embolism or anisohydric behavior are not represented.

Soil hydraulic properties are homogeneous within layers and parameterized using Mualem–van Genuchten function, which may not capture structural heterogeneity, hysteresis, or shrink–swell effects. Numerical integration of the Richards equation uses an explicit adaptive scheme, which may impose stability constraints under extreme gradients. While acknowledging its limitations, the model offers a physically based and sufficiently detailed representation of vertical water fluxes, supporting its use for process-based analysis of soil–plant–atmosphere interactions in this study.

Table S1 Model input parameters - fixed parameters for reference simulations and fixed as well as used ranges of varied parameters during calibration for Kienhorst site

Parameter	Definition	Unit	Param. Ref. Sim.	Fixed param. calibr.	Varied parameters calibration		Source
					Lower bound	Upper bound	
	Meteorologic site parameters						
eslope	Slope of the site	(deg)	0	0			(ICOS_Kie, 2025)
alb	Albedo of soil/vegetation surface without snow	**(-)**	0.13	0.13			(Weis et al., 2023)
albsn	Albedo of soil/vegetation surface with snow	(-)	0.34	0.34			(Weis et al., 2023)
c1	Intercept of linear relation between the ratio of actual to potential solar radiation for the day and sunshine duration	(-)	0.25	0.25			(Weis et al., 2023)
c2	Slope of linear relation between the ratio of actual to potential solar radiation for the day and sunshine duration	(-)	0.5	0.5			(Weis et al., 2023)
c3	Ratio of net longwave radiation for overcast skyto that for clear sky	(-)	0.2	0.2			(Weis et al., 2023)
wndrat	Average ratio of nighttime to daytime wind speed	(-)	0.3	0.3			(Weis et al., 2023)
fetch	Fetch upwind of the weather station at which wind speed was measured	(m)	5000	5000			(Weis et al., 2023)
z0w	Roughness at the weather station where wind speed was measured	(m)	0.005	0.005			(Weis et al., 2023)
zw	The height above the ground at which wind speed (UW) was measured	(m)	10	10			(Weis et al., 2023)
	Canopy parameters						
maxlai	Maximum leaf area index	(m^2 m^{-2})	4.5	4.5			(Weis et al., 2023)
densef	Canopy density	(-)	1	1			
sai	Steam area index	(m^2 m^{-2})	0.8	0.8			(Weis et al., 2023)
age	Canopy age	(year)	119	119			(ICOS_Kie, 2025)
height	Canopy height	(m)	28.3	28.3			(ICOS_Kie, 2025)
lwidth	Average leaf width	(m)	0.001	0.001			(Weis et al., 2023)
z0g	Roughness of the ground surface below the canopy	(m)	0.00325	0.00325			(Weis et al., 2023)
z0s	Roughness parameter of snow surface	(m)	0.001	0.001			(Weis et al., 2023)
lpc	Leaf conductance	(-)	4	4			(Weis et al., 2023)
czs	Ratio of roughness parameter to height when height is less than HS and canopy is closed	(-)	0.13	0.13			(Weis et al., 2023)
czr	Ratio of roughness parameter to height when height is greater than HR and canopy is closed	(-)	0.05	0.05			(Weis et al., 2023)
hs	Short vegetation height threshold	(m)	1	1			(Weis et al., 2023)
hr	Tall vegetation height threshold	(m)	10	10			(Weis et al., 2023)
zminh	Reference height for weather data above canopy	(m)	2	2			(Weis et al., 2023)
rhotp	Ratio of total leaf area to projected area	(-)	2.6	2.6			(Weis et al., 2023)
nn	Wind/diffusivity extinction coefficient	(-)	2.5	2.5			(Weis et al., 2023)
	Interception parameters						
frintlai	Intercepted fraction of rain per unit LAI	(-)	0.13	0.13			(Weis et al., 2023)
fsintlai	Intercepted fraction of snow per unit LAI	(-)	0.13	0.13			(Weis et al., 2023)
frintsai	Intercepted fraction of rain per unit SAI	(-)	0.13	0.13			(Weis et al., 2023)
fsintsai	Intercepted fraction of snow per unit SAI	(-)	0.3	0.3			(Weis et al., 2023)
cintrl	Max. interception storage of rain per LAI	(mm)	1	1			(Weis et al., 2023)
cintrs	Max. interception storage of rain per SAI	(mm)	1	1			(Weis et al., 2023)
cintsl	Max. interception storage of snow water per LAI	(mm)	4	4			(Weis et al., 2023)
cintss	Max. interception storage of snow water per SAI	(mm)	4	4			(Weis et al., 2023)
rstemp	Base temperature for snow-rain transition	(deg)	-0.5	-0.5			(Weis et al., 2023)
	Snowpack parameters						

melfac	Degree-day snowmelt factor for a day with daylength of 0.5 d and no plant canopy	MJ m^{-2} d^{-1} K^{-1}	1.5	1.5			(Weis et al., 2023)
ccfac	Degree day factor for accumulation of cold content for a day with daylength of 0.5 d	MJ m^{-2} d^{-1} K^{-1}	0.3	0.3			(Weis et al., 2023)
laimlt	Dependence of snowmelt on LAI	(-)	0.2	0.2			(Weis et al., 2023)
saimlt	Dependence of snowmelt on SAI	(-)	0.5	0.5			(Weis et al., 2023)
grdmlt	Constant rate of melt at the bottom of the snowpack	(-)	0.35	0.35			(Weis et al., 2023)
maxlqf	Maximum liquid water fraction of snow	(-)	0.05	0.05			(Weis et al., 2023)
ksnvp	Reduction factor to reduce snow evaporation	(-)	0.3	0.3			(Weis et al., 2023)
snoden	Snow density	(mm mm^{-1})	0.3	0.3			(Weis et al., 2023)
	Leaf evaporation parameters						
glmax	Max. leaf vapour conductance when stomata are fully open	(m s^{-1})	0.0045		0.0026	0.0087	(Weis et al., 2023)
glmin	Min. leaf vapour conductance when stomata are closed	(m s^{-1})	0.0002	0.0002			(Weis et al., 2023)
cr	Extinction coefficient for photosy. active radiation in the canopy	(-)	0.45	0.45			(Weis et al., 2023)
rm	Nominal max. solar radiation possible on a leaf	(W m^2)	1000	1000			(Weis et al., 2023)
r5	Solar radiation level at which leaf conductance is half of its value	(W m^2)	100	100			(Weis et al., 2023)
cvpd	Vapor pressure deficit at which stomatal conductance is halved	(kPa)	2		1.5	2.5	(Weis et al., 2023)
tl	Temperature controlling when stomates are closed	(deg)	0	0			(Weis et al., 2023)
t1	Temperature controlling when stomates are closed	(deg)	10	10			(Weis et al., 2023)
t2	Temperatures controlling when stomates are closed	(deg)	30	30			(Weis et al., 2023)
th	Temperatures controlling when stomates are closed	(deg)	40	40			(Weis et al., 2023)
	Plant parameters						
mxkpl	Maximum internal conductivity for water flow through the plants	(mm d^{-1} MPa^{-1})	8	8			(Weis et al., 2023)
mxrtln	Maximum length of fine roots per unit ground area	(m m^{-2})	3000	3000			(Weis et al., 2023)
initrlen	Initial water-absorbing root length per unit area	(m m^{-2})	10	10			(Weis et al., 2023)
initrdep	Initial root depth	(m)	0.25	0.25			(Weis et al., 2023)
rgrorate	Vertical root growth rate	(m a^{-1})	0.033	0.033			(Weis et al., 2023)
rgroper	Period of net root growth	(year)	0	0			(Weis et al., 2023)
fxylem	Fraction of internal plant resistance to water flow that is in the Xylem	(-)	0.5	0.5			(Weis et al., 2023)
psicr	Critical leaf water pot. at which stomates close	(MPa)	-2.5	-2.5			(Weis et al., 2023)
rtrad	Average radius of the fine or water-absorbing roots	(mm)	0.25	0.25			(Weis et al., 2023)
nooutf	Switch to turn ourflow from roots on (0) or off (1)	(-)	1	1			(Weis et al., 2023)
betaroot	β param. of vertical root distribution	(-)	0.976	0.976			(Weis et al., 2023)
maxrootdepth	Maximum root depth	(m)	2	2			(Weis et al., 2023)
	Soil parameters						
idepth	Soil depth until which infiltration is distributed	(m)	1.0	1.0			(ICOS_Kie, 2025)
qdepth	Soil depth until which surface/source area flow is considered	(m)	0.6		0.3	0.9	(ICOS_Kie, 2025)
rssa	Soil evaporation resistance (RSS) at field capacity	(s m^{-1})	100	100			(Weis et al., 2023)
rssb	Exponent in relation of soil evaporation resistance (RSS) to soil water potential (PSIM) in the top layer	(-)	1	1			(Weis et al., 2023)
infexp	Infilt. exponent that determines distribution of infilt. water with depth	(-)	0.6	0.6			(ICOS_Kie, 2025)
bypar	Switch to turn byflow on (1) or off (0)	(-)	0	0			(ICOS_Kie, 2025)
qfpar	Quickflow shape parameter	(-)	2	2			(ICOS_Kie, 2025)
qffc	Quickflow fraction of infiltrating water at field capacity	(-)	0.05	0.05			(ICOS_Kie, 2025)

imperv	Fraction of the soil surface that is impermeable and always routes water reaching it directly to streamflow	(-)	0	0			(Weis et al., 2023)
dslope	Hillslope angle for downslope matric flow	(deg)	0	0			(Weis et al., 2023)
length_slope	Slope length for downslope flow (DSFL)	(m)	0	0			(Weis et al., 2023)
drain	Multiplier to partially activate drainage	(-)	1	1			(Weis et al., 2023)
gsc	Fraction of groundwater storage that is transferred to groundwater flow and deep seepage	(d^{-1})	0	0			(Weis et al., 2023)
gsp	Fraction of groundwater discharge produced by gsc that goes to deep seepage and is not added to streamflow	(-)	0	0			(Weis et al., 2023)
psiini	Initial pressure head of soil layers	(kPa)	-10	-10			(ICOS_Kie, 2025)
ths1	Saturated volumetric soil moisture content – layer1	(-)	0.44		0.35	0.45	(Wösten et al., 1999)
ths2	Saturated volumetric soil moisture content – layer2	(-)	0.43		0.35	0.45	(Wösten et al., 1999)
ths3	Saturated volumetric soil moisture content – layer3	(-)	0.38		0.35	0.45	(Wösten et al., 1999)
thr1	Residual volumetric soil moisture content – layer1	(-)	0.03		0.02	0.05	(Wösten et al., 1999)
thr2	Residual volumetric soil moisture content – layer2	(-)	0.02		0.02	0.05	(Wösten et al., 1999)
thr3	Residual volumetric soil moisture content – layer3	(-)	0.05		0.02	0.05	(Wösten et al., 1999)
alpha1	Alpha parameter of the van Genuchten water retention function - air-entry parameter – layer1	(m^{-1})	6		3	6	(Wösten et al., 1999)
alpha2	Alpha parameter of the van Genuchten water retention function - air-entry parameter – layer2	(m^{-1})	3.6		3	6	(Wösten et al., 1999)
alpha3	Alpha parameter of the van Genuchten water retention function - air-entry parameter- layer3	(m^{-1})	3.45		3	6	(Wösten et al., 1999)
npar1	N parameter of the van Genuchten water retention function - width of the soil's pore-size distribution – layer1	(-)	1.4		1.2	2.5	(Wösten et al., 1999)
npar2	N parameter of the van Genuchten water retention function - width of the soil's pore-size distribution – layer2	(-)	1.56		1.2	2.5	(Wösten et al., 1999)
npar3	N parameter of the van Genuchten water retention function - width of the soil's pore-size distribution – layer3	(-)	2		1.2	2.5	(Wösten et al., 1999)
ksat1	Saturated hydraulic conductivity – layer1	(mm d^{-1})	5419		5000	11000	(Hazen, 1892)
ksat2	Saturated hydraulic conductivity – layer2	(mm d^{-1})	5600		5000	11000	(Hazen, 1892)
ksat3	Saturated hydraulic conductivity – layer3	(mm d^{-1})	10000		5000	11000	(Hazen, 1892)
gravel	Gravel content in the soil	(-)	0	0			measured
tort	Tortuosity parameter of Mualem hydraulic conductivity function	(-)	0.5	0.5			(Mualem, 1976)

Table S2 Model input parameters - fixed parameters for reference simulations and fixed as well as used ranges of varied parameters during calibration for Tharandt site

Parameter	Definition	Unit	Param. Ref. Sim.	Fixed param. calibr.	Varied parameters calibration		Source
					Lower bound	Upper bound	
	Meteorologic site parameters						
eslope	Slope of the site	(deg)	4	4			(ICOS_Tha, 2025)
alb	Albedo of soil/vegetation surface without snow	**(-)**	0.13	0.13			(Weis et al., 2023)
albsn	Albedo of soil/vegetation surface with snow	(-)	0.34	0.34			(Weis et al., 2023)
c1	Intercept of linear relation between the ratio of actual to potential solar radiation for the day and sunshine duration	(-)	0.25	0.25			(Weis et al., 2023)
c2	Slope of linear relation between the ratio of actual to potential solar radiation for the day and sunshine duration	(-)	0.5	0.5			(Weis et al., 2023)
c3	Ratio of net longwave radiation for overcast skyto that for clear sky	(-)	0.2	0.2			(Weis et al., 2023)
wndrat	Average ratio of nighttime to daytime wind speed	(-)	0.3	0.3			(Weis et al., 2023)
fetch	Fetch upwind of the weather station at which wind speed was measured	(m)	5000	5000			(Weis et al., 2023)
z0w	Roughness at the weather station where wind speed was measured	(m)	0.005	0.005			(Weis et al., 2023)
zw	The height above the ground at which wind speed (UW) was measured	(m)	42	42			(ICOS_Tha, 2025)
	Canopy parameters						
maxlai	Maximum leaf area index	(m^2 m^{-2})	7	7			(Weis et al., 2023)
densef	Canopy density	(-)	1	1			(ICOS_Tha, 2025)
sai	Steam area index	(m^2 m^{-2})	1	1			(Weis et al., 2023)
age	Canopy age	(year)	120	120			(ICOS_Tha, 2025)
height	Canopy height	(m)	41	41			(ICOS_Tha, 2025)
lwidth	Average leaf width	(m)	0.001	0.001			(Weis et al., 2023)
z0g	Roughness of the ground surface below the canopy	(m)	0.02	0.02			(Weis et al., 2023)
z0s	Roughness parameter of snow surface	(m)	0.001	0.001			(Weis et al., 2023)
lpc	Leaf conductance	(-)	4	4			(Weis et al., 2023)
czs	Ratio of roughness parameter to height when height is less than HS and canopy is closed	(-)	0.13	0.13			(Weis et al., 2023)
czr	Ratio of roughness parameter to height when height is greater than HR and canopy is closed	(-)	0.05	0.05			(Weis et al., 2023)
hs	Short vegetation height threshold	(m)	1	1			(Weis et al., 2023)
hr	Tall vegetation height threshold	(m)	10	10			(Weis et al., 2023)
zminh	Reference height for weather data above canopy	(m)	2	2			(Weis et al., 2023)
rhotp	Ratio of total leaf area to projected area	(-)	2.6	2.6			(Weis et al., 2023)
nn	Wind/diffusivity extinction coefficient	(-)	2.5	2.5			(Weis et al., 2023)
	Interception parameters						
frintlai	Intercepted fraction of rain per unit LAI	(-)	0.08	0.08			(Weis et al., 2023)
fsintlai	Intercepted fraction of snow per unit LAI	(-)	0.08	0.08			(Weis et al., 2023)
frintsai	Intercepted fraction of rain per unit SAI	(-)	0.08	0.08			(Weis et al., 2023)
fsintsai	Intercepted fraction of snow per unit SAI	(-)	0.1	0.1			(Weis et al., 2023)
cintrl	Max. interception storage of rain per LAI	(mm)	0.4	0.4			(Weis et al., 2023)
cintrs	Max. interception storage of rain per SAI	(mm)	0.2	0.2			(Weis et al., 2023)
cintsl	Max. interception storage of snow water per LAI	(mm)	1.6	1.6			(Weis et al., 2023)
cintss	Max. interception storage of snow water per SAI	(mm)	0.8	0.8			(Weis et al., 2023)
rstemp	Base temperature for snow-rain transition	(deg)	-0.5	-0.5			(Weis et al., 2023)

	Snowpack parameters						
melfac	Degree-day snowmelt factor for a day with daylength of 0.5 d and no plant canopy	MJ m^{-2} d^{-1} K^{-1}	1.5	1.5			(Weis et al., 2023)
ccfac	Degree day factor for accumulation of cold content for a day with daylength of 0.5 d	MJ m^{-2} d^{-1} K^{-1}	0.3	0.3			(Weis et al., 2023)
laimlt	Dependence of snowmelt on LAI	(-)	0.2	0.2			(Weis et al., 2023)
saimlt	Dependence of snowmelt on SAI	(-)	0.5	0.5			(Weis et al., 2023)
grdmlt	Constant rate of melt at the bottom of the snowpack	(-)	0.35	0.35			(Weis et al., 2023)
maxlqf	Maximum liquid water fraction of Snow	(-)	0.05	0.05			(Weis et al., 2023)
ksnvp	Reduction factor to reduce snow evaporation	(-)	0.03	0.03			(Weis et al., 2023)
snoden	Snow density	(mm mm^{-1})	0.3	0.3			(Weis et al., 2023)
	Leaf evaporation parameters						
glmax	Max. leaf vapour conductance when stomata are fully open	(m s^{-1})	0.0035		0.0025	0.0075	(Weis et al., 2023)
glmin	Min. leaf vapour conductance when stomata are closed	(m s^{-1})	0.0001	0.0001			(Weis et al., 2023)
cr	Extinction coefficient for photosy. active radiation in the canopy	(-)	0.45	0.45			(Weis et al., 2023)
rm	Nominal max. solar radiation possible on a leaf	(W m^2)	1000	1000			(Weis et al., 2023)
r5	Solar radiation level at which leaf conductance is half of its value	(W m^2)	100	100			(Weis et al., 2023)
cvpd	Vapor pressure deficit at which stomatal conductance is halved	(kPa)	2		1.5	2.5	(Weis et al., 2023)
tl	Temperature controlling when stomates are closed	(deg)	0	0			(Weis et al., 2023)
t1	Temperature controlling when stomates are closed	(deg)	10	10			(Weis et al., 2023)
t2	Temperatures controlling when stomates are closed	(deg)	30	30			(Weis et al., 2023)
th	Temperatures controlling when stomates are closed	(deg)	40	40			(Weis et al., 2023)
	Plant parameters						
mxkpl	Maximum internal conductivity for water flow through the plants	(mm d^{-1} MPa^{-1})	8	8			(Weis et al., 2023)
mxrtln	Maximum length of fine roots per unit ground area	(m m^{-2})	3000	3000			(Weis et al., 2023)
initrlen	Initial water-absorbing root length per unit area	(m m^{-2})	10	10			(Weis et al., 2023)
initrdep	Initial root depth	(m)	0.25	0.25			(Weis et al., 2023)
rgrorate	Vertical root growth rate	(m a^{-1})	0.033	0.033			(Weis et al., 2023)
rgroper	Period of net root growth	(year)	0	0			(Weis et al., 2023)
fxylem	Fraction of internal plant resistance to water flow that is in the Xylem	(-)	0.5	0.5			(Weis et al., 2023)
psicr	Critical leaf water pot. at which stomates close	(MPa)	-2	-2			(Weis et al., 2023)
rtrad	Average radius of the fine or water-absorbing roots	(mm)	0.25	0.25			(Weis et al., 2023)
nooutf	Switch to turn ourflow from roots on (0) or off (1)	(-)	1	1			(Weis et al., 2023)
betaroot	β param. of vertical root distribution	(-)	0.976				(Weis et al., 2023)
maxrootdepth	Maximum root depth	(m)	- 1.2				(Weis et al., 2023)
	Soil parameters						
idepth	Soil depth until which infiltration is distributed	(m)	0.6		0	1	(ICOS_Tha, 2025)
qdepth	Soil depth until which surface/source area flow is considered	(m)	0	0			(ICOS_Tha, 2025)
rssa	Soil evaporation resistance (RSS) at field capacity	(s m^{-1})	100	100			(Weis et al., 2023)
rssb	Exponent in relation of soil evaporation resistance (RSS) to soil water potential (PSIM) in the top layer	(-)	1	1			(Weis et al., 2023)
infexp	Infilt. exponent that determines distribution of infilt. water with depth	(-)	0.5		0.2	1	(ICOS_Tha, 2025)
bypar	Switch to turn byflow on (1) or off (0)	(-)	1	1			(ICOS_Tha, 2025)
qfpar	Quickflow shape parameter	(-)	0.25		0	0.5	(ICOS_Tha, 2025)

qffc	Quickflow fraction of infiltrating water at field capacity	(-)	0.25		0.1	0.5	(ICOS_Tha, 2025)
imperv	Fraction of the soil surface that is impermeable and always routes water reaching it directly to streamflow	(-)	0	0			(Weis et al., 2023)
dslope	Hillslope angle for downslope matric flow	(deg)	0	0			(Weis et al., 2023)
length_slope	Slope length for downslope flow (DSFL)	(m)	0	0			(Weis et al., 2023)
drain	Multiplier to partially activate drainage	(-)	1	1			(Weis et al., 2023)
gsc	Fraction of groundwater storage that is transferred to groundwater flow and deep seepage	(d^{-1})	0	0			(Weis et al., 2023)
gsp	Fraction of groundwater discharge produced by gsc that goes to deep seepage and is not added to streamflow	(-)	0	0			(Weis et al., 2023)
psiini	Initial pressure head of soil layers	(kPa)	-10	-10			(ICOS_Tha, 2025)
ths1	Saturated volumetric soil moisture content – layer1	(-)	0.55		0.4	0.6	(Wösten et al., 1999)
ths2	Saturated volumetric soil moisture content – layer2	(-)	0.45		0.4	0.6	(Wösten et al., 1999)
ths3	Saturated volumetric soil moisture content – layer3	(-)	0.41		0.4	0.6	(Wösten et al., 1999)
thr1	Residual volumetric soil moisture content – layer1	(-)	0.12		0.04	0.14	(Wösten et al., 1999)
thr2	Residual volumetric soil moisture content – layer2	(-)	0.05		0.04	0.14	(Wösten et al., 1999)
thr3	Residual volumetric soil moisture content – layer3	(-)	0.07		0.04	0.14	(Wösten et al., 1999)
alpha1	Alpha parameter of the van Genuchten water retention function - air-entry parameter – layer1	(m^{-1})	3		2	5	(Wösten et al., 1999)
alpha2	Alpha parameter of the van Genuchten water retention function - air-entry parameter – layer2	(m^{-1})	3		2	5	(Wösten et al., 1999)
alpha3	Alpha parameter of the van Genuchten water retention function - air-entry parameter- layer3	(m^{-1})	3.7		2	5	(Wösten et al., 1999)
npar1	N parameter of the van Genuchten water retention function - width of the soil's pore-size distribution – layer1	(-)	1.5		1.2	2.5	(Wösten et al., 1999)
npar2	N parameter of the van Genuchten water retention function - width of the soil's pore-size distribution – layer2	(-)	1.2		1.2	2.5	(Wösten et al., 1999)
npar3	N parameter of the van Genuchten water retention function - width of the soil's pore-size distribution – layer3	(-)	1.5		1.2	2.5	(Wösten et al., 1999)
ksat1	Saturated hydraulic conductivity – layer1	(mm d^{-1})	1000		100	1200	(Hazen, 1892)
ksat2	Saturated hydraulic conductivity – layer2	(mm d^{-1})	730		100	1200	(Hazen, 1892)
ksat3	Saturated hydraulic conductivity – layer3	(mm d^{-1})	294		100	1200	(Hazen, 1892)
gravel1	Gravel content in the soil – layer1	(-)	0.48		0	0.7	measured
gravel2	Gravel content in the soil – layer2	(-)	0.48		0	0.7	measured
gravel3	Gravel content in the soil – layer3	(-)	0.63		0	0.7	measured
tort	Tortuosity parameter of Mualem hydraulic conductivity function	(-)	0.5	0.5			(Mualem, 1976)

Satistics

Evaluation of model performance

The Kling–Gupta efficiency (KGE), a metric used to evaluate the accuracy and quality of models that simulate hydrologic processes (Knoben et al., 2019) was used as model performance criteria. It enhances traditional efficiency measures by integrating three key statistical components: correlation, variability bias, and mean bias. The KGE provides a more balanced assessment of model performance by considering not only the strength of the linear relationship but also the distribution and scale differences between observed and simulated values and its formula was proposed by (Gupta et al., 2009):

$$KGE = 1 - \sqrt{(r-1)^2 + \left(\frac{\sigma_{sim}}{\sigma_{obs}} - 1\right)^2 + \left(\frac{\mu_{sim}}{\mu_{obs}} - 1\right)^2} \quad \text{(S1)}$$

where σ_obsand σ_sim denote the standard deviations of observations and simulationsand μ_sim and μ_obs their respective means. Regarding the interpretation of KGE values, KGE = 1 signifies a perfect match between simulations and observations. A KGE value close to 1 reflects strong correspondence between simulated and observed data. However, KGE < 0 suggests that the mean of observations may provide more accurate estimates than simulations, indicating a poor fit (Castaneda-Gonzalez et al., 2018; Koskinen et al., 2017), where the model performs worse than using the mean as a prediction (Andersson et al., 2017; Schönfelder et al., 2017). The three components of the KGE capture distinct aspects of model performance:

Correlation (r):
It reflects how well the model reproduces the temporal dynamics and timing of fluctuations. High correlation (r = 0.8 – 1.0) indicates that the model captures the sequence and co-variation of hydrological responses, even if magnitudes differ.

Variability bias (σ_sim / σ_obs):
Quantifies the model's ability to reproduce the amplitude of variability in the observations. A ratio of 1 indicates that the simulated variability matches the observed spread; values >1 or <1 indicate over- or underestimation of variability, respectively. This component is particularly relevant for assessing whether the model captures the intensity of wetting–drying cycles or event-driven dynamics.

Mean bias (μ_sim / μ_obs):

Represents systematic differences in the average magnitude of simulated versus observed values. A ratio of 1 indicates unbiased mean conditions, whereas deviations reflect persistent over- or underestimation. This component is essential for evaluating long-term water balance consistency.

Variation of parameters

The coefficient of variation (CV) was computed as a normalized measure of dispersion. The CV, defined as the ratio of the plotard deviation to the mean, enables comparison of variability across parameters with different magnitudes and units. Parameters exhibiting elevated coefficient of variation (CV) values were recognized as highly variable, suggesting the need for detailed analysis of their impact on model performance and sensitivity (Fowler et al., 1998).

Monte-Carlo Subsampling

To determine the number of spatial samples required for a representative estimate of a hydrological variable, a Monte-Carlo subsampling framework can be applied. This approach evaluates how aggregated estimates change as a function of sample size and provides a data-driven basis for identifying the minimum number of samples needed to capture spatial variability (Davison and Hinkley, 1997; Efron and Tibshirani, 1994; Manly and Manly, 2018). Given a set of *N* spatial units with associated hydrological estimates R_i, random subsets of size

$$k \in \{1, \dots, N\} \tag{S2}$$

are repeatedly drawn. For each subset S_k, an aggregated estimate is computed as

$$R_{S_k} = \frac{1}{k} \sum_{i \in S_k} R_i \tag{S3}$$

Iterating this procedure yields empirical distributions of R_{S_k} for each sample size. Representativeness can be assessed by comparing these distributions to the full-ensemble estimate μ_{full}, for example by requiring that the relative deviation of the subsample mean remains within a predefined tolerance δ:

$$\left| \frac{E\left[R_{S_k}\right] - \mu_{full}}{\mu_{full}} \right| \leq \delta \tag{S4}$$

Additional criteria, such as overlap of confidence intervals, can be used to ensure that both central tendency and distributional characteristics are preserved. Because this method relies on repeated random sampling rather than assumptions of independence or spatial homogeneity, it is broadly applicable to heterogeneous hydrological systems.

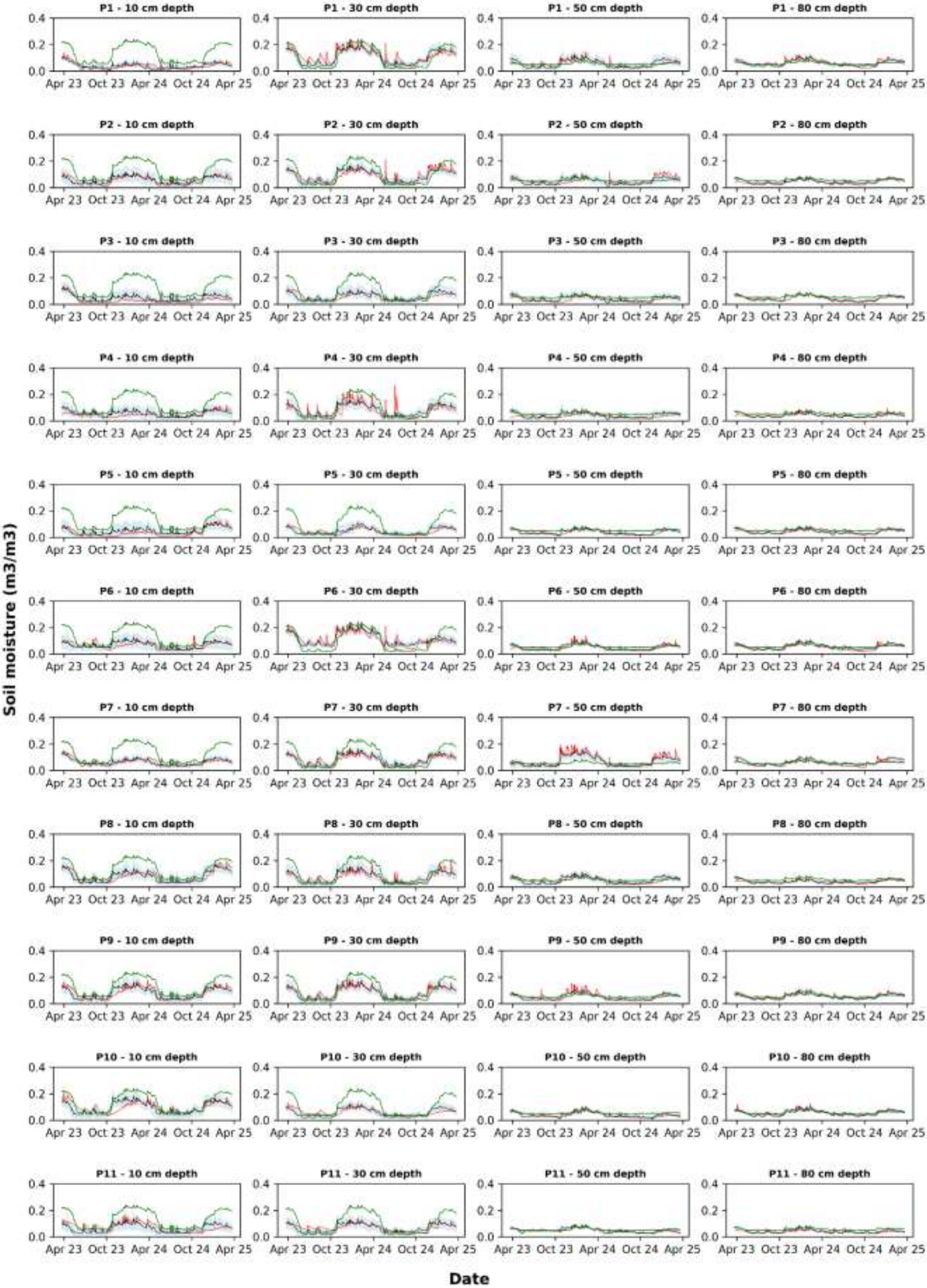

Figure S1 Soil moisture - Observed (red) versus reference simulation (green) as well as average of the 30 best calibrated simulations (black) and their uncertainty bandwidth (blue) for profile 1 to 11 in the depths 10, 30, 50 and 80 cm at Kienhorst plot

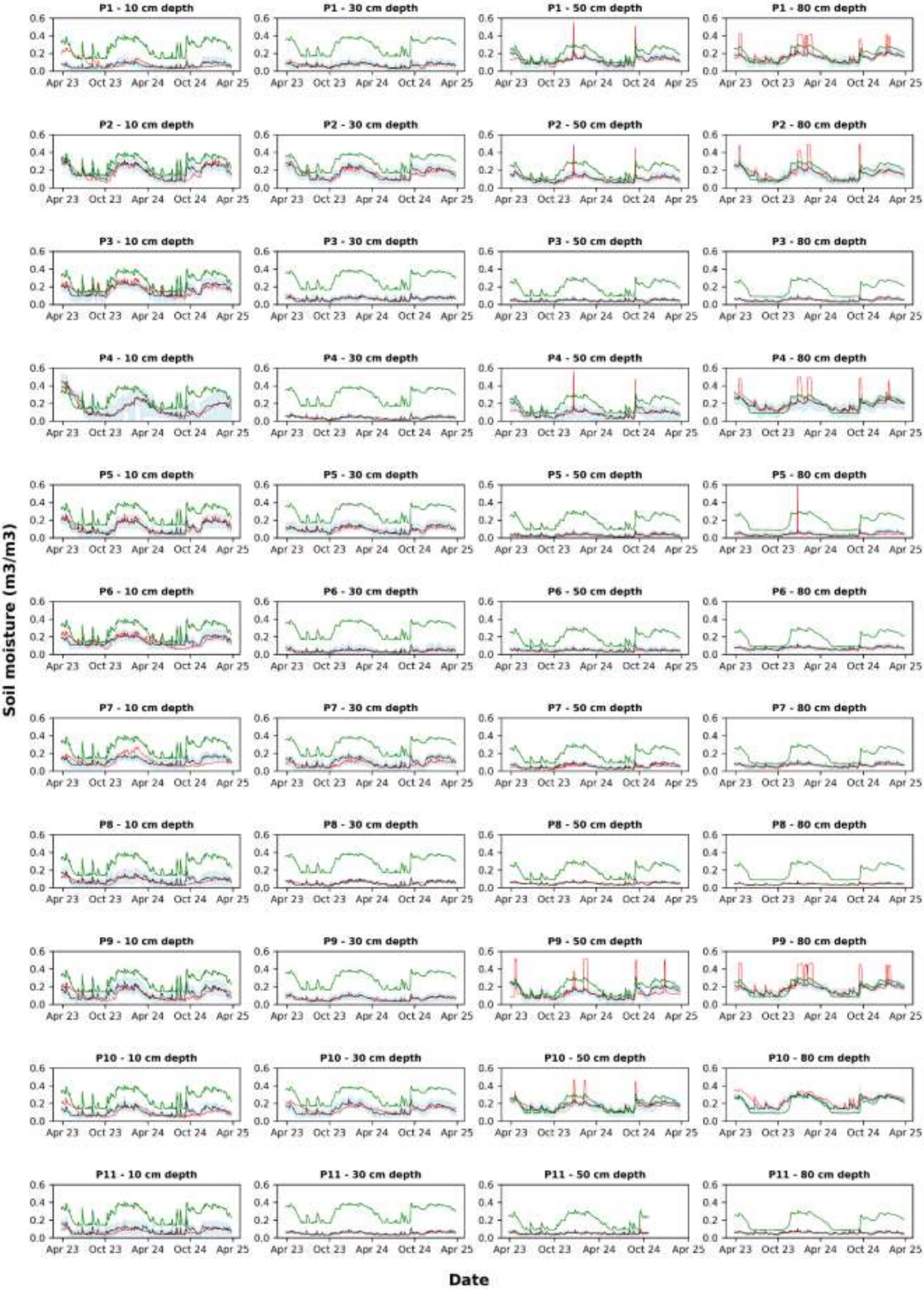

Figure S2 Soil moisture **-** Observed (red) versus reference simulations (green) as well as average of the 30 best calibrated simulations (black) and their uncertainty bandwidth (blue) for profile 1 to 11 in the depths 10, 30, 50 and 80 cm at Tharandt plot

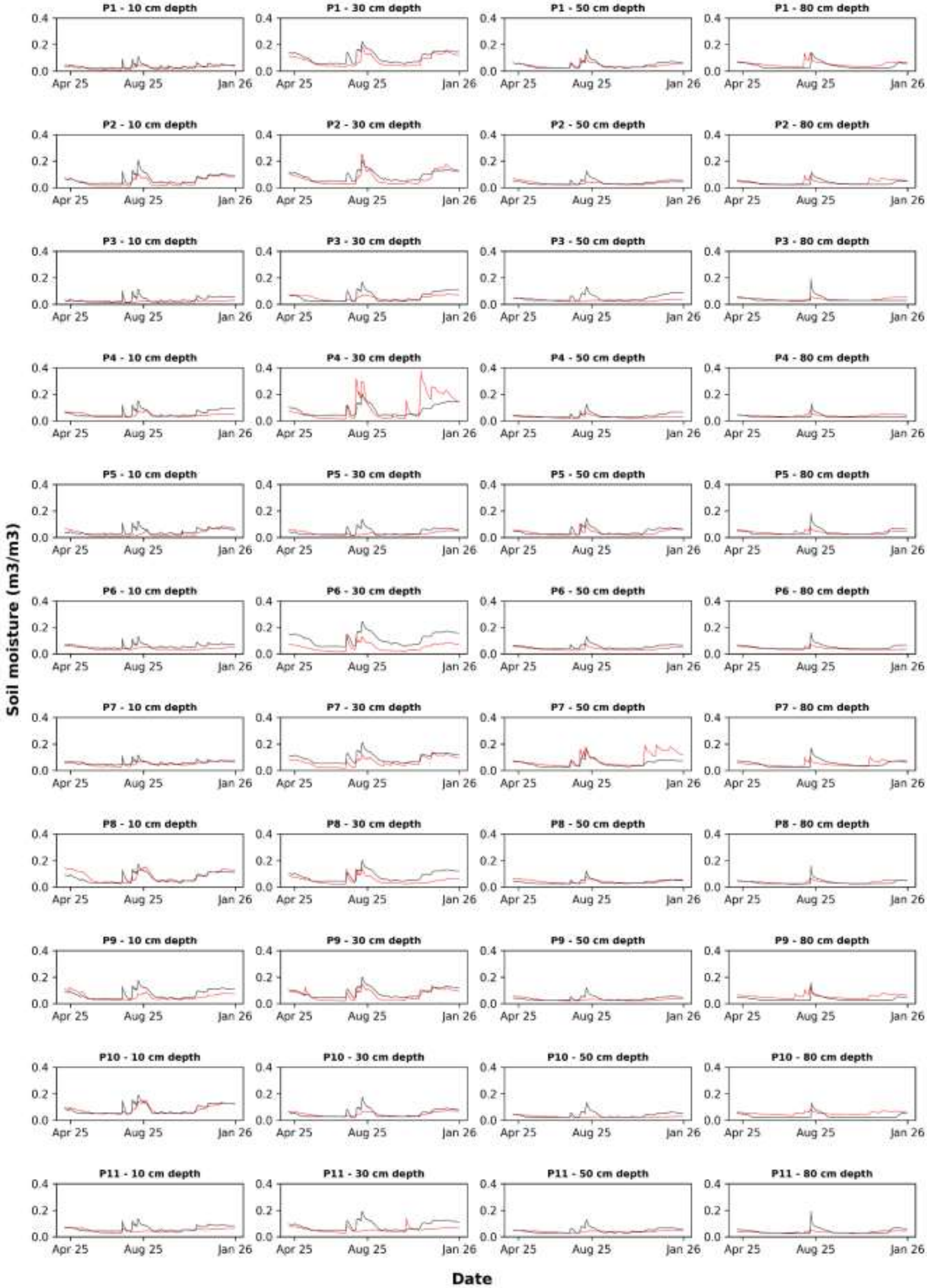

Figure S3 Soil moisture - Observed (red) versus simulated (black) based on the best parameter set of the 30 best simulatins during validation period for profile 1 to 11 in the depths 10, 30, 50 and 80 cm at Kienhorst plot

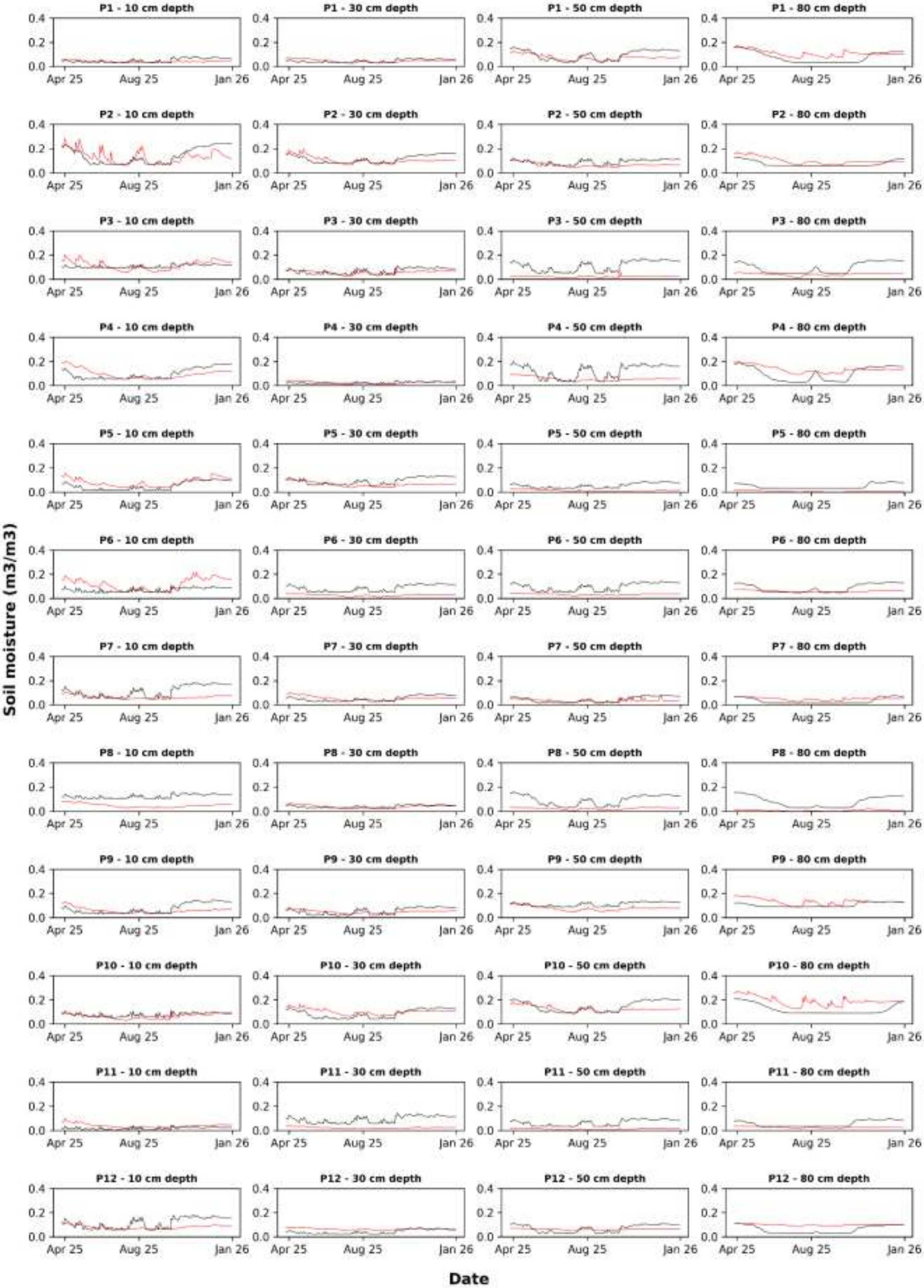

Figure S4 Soil moisture - Observed (red) versus simulated (black) based on the best parameter set of the 30 best simulatins during validation period for profile 1 to 11 in the depths 10, 30, 50 and 80 cm at Tharandt plot

Table S3 Kling Gupta efficiency for agreement between observed and simulated soil moisture for reference simulation (*), average of the 30 best calibrated simulations (**) as well as validated simulations (***) at Kienhorst plot

Depth		**P 1**	**P 2**	**P 3**	**P 4**	**P 5**	**P 6**	**P 7**	**P 8**	**P 9**	**P 10**	**P 11**
	ref. – obs.*	-2.10	-0.78	-2.86	-2.09	-1.75	-1.31	-1.01	0.15	0.13	0.09	-0.32
10 cm	sim. – obs.**	0.69	0.80	0.39	0.56	0.59	0.56	0.79	0.82	0.83	0.61	0.55
	val. – obs.***	0.43	0.57	-1.10	-0.06	0.36	0.08	0.54	0.70	0.34	0.76	0.15
	ref. – obs.*	0.30	0.13	-1.38	0.30	-1.91	0.27	-0.30	-0.26	0.02	-1.39	-1.24
30 cm	sim. – obs.**	0.82	0.84	0.66	0.69	0.76	0.87	0.85	0.83	0.94	0.69	0.70
	val. – obs.***	0.64	0.64	-0.10	0.39	-0.16	-0.42	0.55	0.16	0.71	0.14	-0.38
	ref. – obs.*	0.29	0.06	0.21	0.28	0.25	0.30	0.07	0.33	0.24	0.27	0.52
50 cm	sim. – obs.**	0.71	0.67	0.61	0.12	0.74	0.85	0.77	0.63	0.73	0.82	0.65
	val. – obs.***	0.47	0.25	-0.91	-0.07	0.46	0.21	0.38	0.57	0.01	-2.09	-0.95
	ref. – obs.*	0.35	0.35	0.37	0.50	0.40	0.37	0.45	0.47	0.52	0.50	0.41
80 cm	sim. – obs.**	0.84	0.79	0.76	0.65	0.74	0.81	0.62	0.59	0.66	0.75	0.41
	val. – obs.***	0.44	0.26	-0.09	-0.06	-0.34	0.13	0.26	0.39	0.28	-0.10	-0.81

Table S4 Correlation component of Kling Gupta efficiency for agreement between observed and simulated soil moisture for reference simulation (*), average of the 30 best calibrated simulations (**) as well as validated simulations (***) at Kienhorst plot

Depth		**P 1**	**P 2**	**P 3**	**P 4**	**P 5**	**P 6**	**P 7**	**P 8**	**P 9**	**P 10**	**P 11**
	ref. – obs.*	0.73	0.88	0.54	0.54	0.57	0.62	0.74	0.83	0.94	0.81	0.77
10 cm	sim. – obs.**	0.78	0.86	0.83	0.59	0.84	0.57	0.82	0.84	0.85	0.66	0.59
	val. – obs.***	0.60	0.87	0.48	0.54	0.53	0.28	0.59	0.76	0.63	0.89	0.46
	ref. – obs.*	0.84	0.78	0.87	0.76	0.83	0.74	0.85	0.87	0.86	0.86	0.85
30 cm	sim. – obs.**	0.86	0.85	0.68	0.81	0.78	0.90	0.90	0.85	0.94	0.70	0.76
	val. – obs.***	0.92	0.91	0.77	0.78	0.38	0.90	0.86	0.77	0.90	0.77	0.42
	ref. – obs.*	0.78	0.37	0.78	0.75	0.76	0.86	0.70	0.78	0.82	0.81	0.77
50 cm	sim. – obs.**	0.82	0.67	0.68	0.58	0.75	0.86	0.94	0.73	0.85	0.85	0.77
	val. – obs.***	0.86	0.51	0.20	0.54	0.70	0.81	0.76	0.62	0.29	-0.11	0.45
	ref. – obs.*	0.83	0.85	0.80	0.81	0.79	0.84	0.80	0.76	0.86	0.91	0.75
80 cm	sim. – obs.**	0.85	0.86	0.88	0.72	0.88	0.87	0.82	0.73	0.88	0.92	0.81
	val. – obs.***	0.54	0.27	0.40	0.26	0.63	0.62	0.39	0.59	0.38	0.36	0.59

Table S5 Variability bias component of Kling Gupta efficiency for agreement between observed and simulated soil moisture for reference simulation (*), average of the 30 best calibrated simulations (**) as well as validated simulations (***) at Kienhorst plot

Depth		**P 1**	**P 2**	**P 3**	**P 4**	**P 5**	**P 6**	**P 7**	**P 8**	**P 9**	**P 10**	**P 11**
	ref. – obs.*	3.56	2.25	4.43	2.72	3.48	1.96	2.06	1.64	1.68	1.34	1.87
10 cm	sim. – obs.**	0.79	0.86	0.93	1.07	0.76	1.11	0.90	0.92	0.91	1.19	0.84
	val. – obs.***	1.14	1.13	2.83	1.91	0.86	1.38	0.84	0.85	1.39	1.21	1.57
	ref. – obs.*	0.90	1.15	1.90	1.37	2.36	0.95	1.34	1.44	1.25	1.76	1.47
30 cm	sim. – obs.**	1.10	0.96	1.03	0.76	1.05	0.95	1.09	1.03	1.02	1.07	1.18
	val. – obs.***	1.07	0.76	2.07	0.46	1.91	1.67	1.04	1.43	1.00	1.82	2.14
	ref. – obs.*	1.01	1.06	1.54	1.59	1.45	1.15	0.70	1.04	1.02	1.34	1.15
50 cm	sim. – obs.**	1.22	0.95	1.17	1.74	1.03	0.96	0.83	1.26	0.79	0.90	1.26
	val. – obs.***	1.50	1.54	2.63	1.93	1.35	1.63	0.52	1.19	1.65	3.86	2.87
	ref. – obs.*	0.93	1.44	1.36	1.42	1.44	1.16	1.13	1.44	1.03	0.98	1.54
80 cm	sim. – obs.**	0.96	0.98	1.19	1.22	1.20	0.98	1.21	1.30	1.32	1.23	1.55
	val. – obs.***	1.21	1.05	1.91	1.71	2.29	1.72	1.41	1.44	1.05	1.79	2.75

Table S6 Mean bias component of Kling Gupta efficiency for agreement between observed and simulated soil moisture for reference simulation (*), average of the 30 best calibrated simulations (**) as well as validated simulations (***) at Kienhorst plot

Depth		**P 1**	**P 2**	**P 3**	**P 4**	**P 5**	**P 6**	**P 7**	**P 8**	**P 9**	**P 10**	**P 11**
	ref. – obs.*	2.72	2.27	2.70	3.53	2.10	3.06	2.68	1.52	1.53	1.82	1.97
10 cm	sim. – obs.**	1.07	0.96	1.59	1.14	1.29	0.99	1.00	1.00	1.01	0.96	0.92
	val. – obs.***	1.39	1.39	1.89	1.29	1.41	1.43	1.14	0.90	1.38	1.03	1.33
	ref. – obs.*	1.68	1.83	3.20	1.55	3.57	1.69	2.24	2.17	1.93	3.27	3.18
30 cm	sim. – obs.**	0.94	0.97	1.11	1.06	1.07	1.05	1.07	1.07	1.01	1.06	0.97
	val. – obs.***	1.34	1.25	1.13	0.83	1.36	2.24	1.43	1.69	1.28	1.13	1.52
	ref. – obs.*	0.32	0.31	0.48	0.68	0.45	0.33	0.17	0.37	0.26	0.38	0.60
50 cm	sim. – obs.**	1.05	0.96	1.15	1.22	1.06	1.05	0.87	0.99	0.94	0.99	1.01
	val. – obs.***	1.10	1.15	1.61	1.27	1.27	1.44	0.69	0.91	1.25	1.37	1.13
	ref. – obs.*	0.38	0.54	0.52	0.81	0.66	0.42	0.50	0.84	0.54	0.51	1.04
80 cm	sim. – obs.**	1.00	1.16	1.07	1.01	1.10	1.14	1.26	1.06	1.02	0.96	1.12
	val. – obs.***	0.77	0.88	0.94	0.77	1.02	1.30	1.03	0.95	0.64	0.57	1.17

Table S7 Kling Gupta efficiency for agreement between observed and simulated soil moisture for reference simulation (*), average of the 30 best calibrated simulations (**) as well as validated simulations (***) at Tharandt plot

Depth		**P 1**	**P 2**	**P 3**	**P 4**	**P 5**	**P 6**	**P 7**	**P 8**	**P 9**	**P 10**	**P 11**
	ref. – obs.*	-1.45	0.44	0.17	0.02	-0.24	-0.02	-0.52	-2.29	-0.53	-0.92	-3.03
10 cm	sim. – obs.**	0.18	0.77	0.73	0.90	0.87	0.56	0.43	0.57	0.62	0.47	0.45
	val. – obs.***	-0.51	0.48	0.18	0.28	0.56	0.18	-1.54	-0.87	-0.25	0.50	-0.09
	ref. – obs.*	-3.63	-0.07	-4.52	-7.70	-2.41	-9.32	-2.40	-4.88	-3.45	-0.81	-6.92
30 cm	sim. – obs.**	0.61	0.78	0.60	0.64	0.49	0.16	0.21	0.64	0.76	0.50	0.54
	val. – obs.***	0.24	0.42	0.27	0.23	0.02	-2.52	0.15	0.41	-0.37	0.21	-3.77
	ref. – obs.*	0.04	-0.27	-8.92	-0.51	-7.70	-8.56	-3.97	-6.19	0.29	0.53	-8.76
50 cm	sim. – obs.**	0.66	0.67	0.25	0.53	0.61	0.21	0.41	0.43	0.33	0.58	0.14
	val. – obs.***	-0.06	0.19	-9.10	-1.52	-3.04	-4.66	-0.30	-4.21	0.24	-0.15	-5.91
	ref. – obs.*	0.64	0.60	-5.99	0.60	-3.42	-4.90	-3.96	-13.50	0.57	0.61	-9.68
80 cm	sim. – obs.**	0.35	0.57	0.43	0.39	0.21	0.68	0.65	0.34	0.35	0.81	0.28
	val. – obs.***	0.21	0.53	-2.63	-0.09	-7.38	-2.16	-0.26	-13.2	0.24	0.55	-3.29

Table S8 Correlation component of Kling Gupta efficiency for agreement between observed and simulated soil moisture for reference simulation (*), average of the 30 best calibrated simulations (**) as well as validated simulations (***) at Tharandt plot

Depth		**P 1**	**P 2**	**P 3**	**P 4**	**P 5**	**P 6**	**P 7**	**P 8**	**P 9**	**P 10**	**P 11**
	ref. – obs.*	0.11	0.78	0.76	0.38	0.81	0.65	0.55	0.63	0.73	0.59	0.83
10 cm	sim. – obs.**	0.02	0.84	0.74	0.91	0.90	0.67	0.50	0.67	0.65	0.50	0.76
	val. – obs.***	0.13	0.58	0.50	0.33	0.82	0.66	0.28	0.06	0.23	0.68	0.16
	ref. – obs.*	0.72	0.76	0.89	0.67	0.84	0.86	0.87	0.83	0.86	0.73	0.87
30 cm	sim. – obs.**	0.71	0.87	0.73	0.66	0.83	0.65	0.87	0.70	0.81	0.62	0.74
	val. – obs.***	0.24	0.43	0.55	0.29	0.27	0.51	0.23	0.45	0.40	0.57	0.28
	ref. – obs.*	0.63	0.59	0.80	0.60	0.83	0.89	0.86	0.83	0.56	0.64	0.91
50 cm	sim. – obs.**	0.69	0.75	0.66	0.63	0.73	0.50	0.84	0.60	0.51	0.70	0.61
	val. – obs.***	0.65	0.32	0.67	0.48	0.08	0.44	0.50	0.90	0.39	0.50	0.58
	ref. – obs.*	0.66	0.61	0.83	0.68	0.29	0.88	0.83	0.72	0.66	0.87	0.82
80 cm	sim. – obs.**	0.68	0.74	0.84	0.72	0.37	0.77	0.76	0.62	0.70	0.86	0.63
	val. – obs.***	0.69	0.68	0.78	0.67	0.30	0.58	0.52	0.73	0.33	0.76	0.28

Table S9 Variability bias component of Kling Gupta efficiency for agreement between observed and simulated soil moisture for reference simulation (*), average of the 30 best calibrated simulations (**) as well as validated simulations (***) at Tharandt plot

Depth		P 1	P 2	P 3	P 4	P 5	P 6	P 7	P 8	P 9	P 10	P 11
	ref. – obs.*	1.63	1.12	1.56	1.03	1.44	1.60	1.57	3.09	1.60	1.89	3.69
10 cm	sim. – obs.**	0.44	0.85	0.92	1.08	0.91	0.70	0.68	1.20	0.98	0.85	1.35
	val. – obs.***	2.25	1.27	0.34	1.19	1.03	0.37	3.29	1.02	2.01	0.70	0.66
	ref. – obs.*	4.35	1.63	5.34	5.88	3.59	8.37	2.99	4.80	4.06	2.36	7.31
30 cm	sim. – obs.**	1.16	1.17	1.20	1.17	1.55	1.79	1.89	1.39	1.26	1.32	1.45
	val. – obs.***	1.00	1.07	1.54	0.71	1.49	3.71	1.35	0.80	2.23	1.64	4.30
	ref. – obs.*	1.61	1.80	10.29	1.72	6.81	9.83	4.73	7.64	0.75	1.28	10.31
50 cm	sim. – obs.**	0.85	0.74	1.73	1.08	1.28	1.69	1.54	1.39	0.54	0.71	1.76
	val. – obs.***	1.96	1.26	10.21	3.17	2.95	6.31	2.18	5.04	0.98	2.02	5.79
	ref. – obs.*	0.89	0.95	7.42	0.81	2.77	6.67	5.56	15.06	0.75	1.25	11.43
80 cm	sim. – obs.**	0.45	0.70	1.51	0.47	0.69	1.20	1.16	1.50	0.41	0.95	1.69
	val. – obs.***	1.67	0.79	4.36	2.00	4.71	4.09	2.11	9.30	0.69	1.11	5.07

Table S10 Mean bias component of Kling Gupta efficiency for agreement between observed and simulated soil moisture for reference simulation (*), average of the 30 best calibrated simulations (**) as well as validated simulations (***) at Tharandt plot

Depth		P 1	P 2	P 3	P 4	P 5	P 6	P 7	P 8	P 9	P 10	P 11
	ref. – obs.*	3.20	1.49	1.57	1.76	2.14	1.75	2.34	3.50	2.38	2.66	4.00
10 cm	sim. – obs.**	0.77	1.08	0.93	1.09	0.91	1.06	1.07	1.28	1.13	1.06	1.21
	val. – obs.***	1.25	1.06	0.91	1.00	0.62	0.59	1.74	2.60	1.25	1.19	0.43
	ref. – obs.*	4.19	1.82	4.41	8.20	3.22	8.23	3.76	5.48	4.23	2.17	5.79
30 cm	sim. – obs.**	0.90	1.05	0.91	1.09	1.05	1.26	1.32	1.03	0.91	0.92	1.09
	val. – obs.***	1.01	1.09	1.18	0.90	1.43	3.19	0.94	1.08	1.10	0.83	4.36
	ref. – obs.*	1.64	1.89	4.48	2.27	7.47	4.65	4.28	3.75	1.50	1.13	3.92
50 cm	sim. – obs.**	1.14	1.08	1.09	1.18	1.23	1.27	1.232	1.05	1.02	1.06	1.20
	val. – obs.***	1.27	1.34	5.12	2.15	4.42	2.87	1.25	4.29	1.45	1.18	5.96
	ref. – obs.*	1.00	1.06	3.78	0.86	4.98	2.61	2.96	4.52	0.91	0.73	3.29
80 cm	sim. – obs.**	0.81	0.86	1.05	0.91	1.14	1.05	1.16	1.09	0.83	0.88	1.05
	val. – obs.***	0.71	0.74	2.36	0.74	8.48	1.49	0.67	12.54	0.79	0.63	2.16

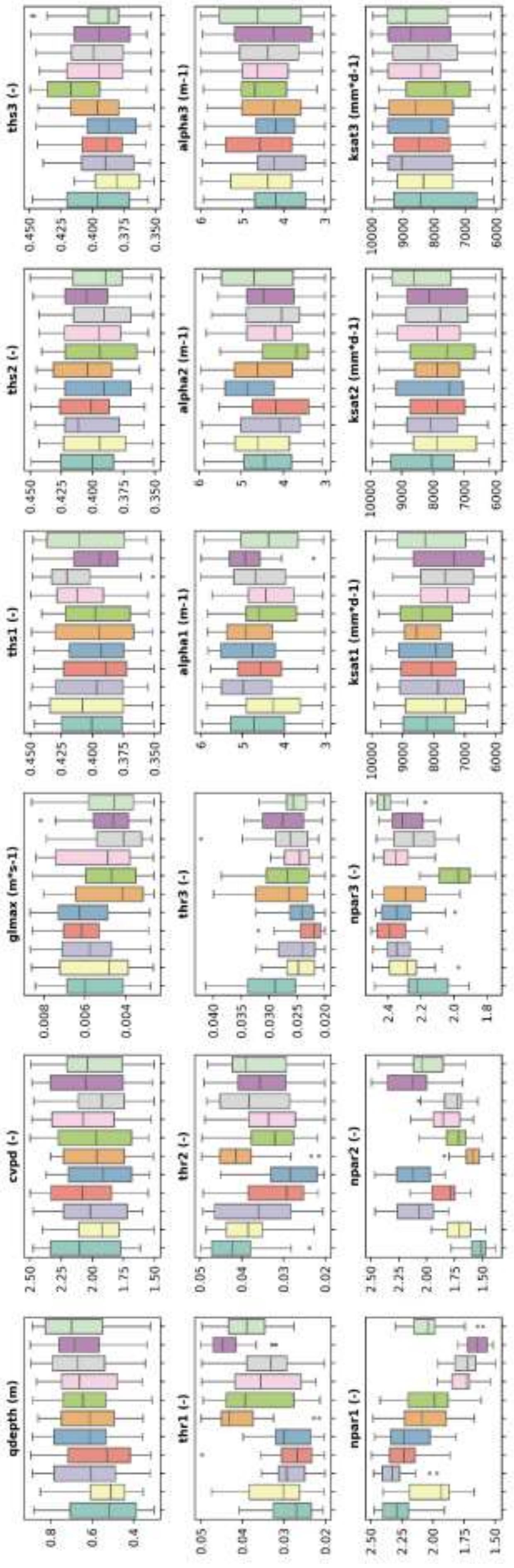

Figure S5 Variation of the input parameters for the individual 11 soil profiles each based on the 30 best simulations for Kienhorst plot

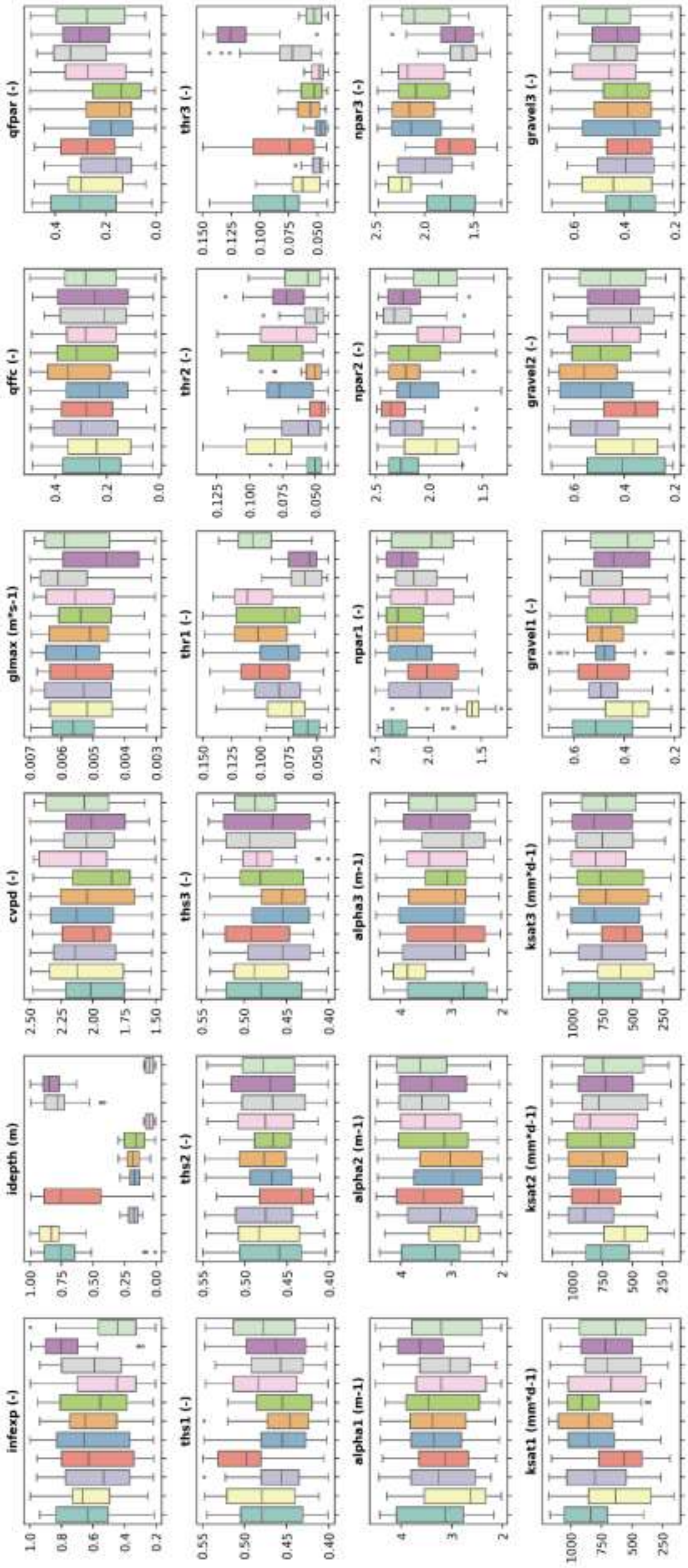

Figure S6 Variation of the input parameters in the individual 11 soil profiles each based on the 30 best simulations for Tharandt plot

Table S11 Determined parameter sets for Kienhorst plot – mean of the 30 best simulation related to KGE

	P 1	P 2	P 3	P 4	P 5	P 6	P 7	P 8	P 9	P 10	P11
qdepth	0.55	0.54	0.62	0.57	0.64	0.62	0.62	0.63	0.66	0.65	0.67
cvpd	2.06	1.94	2.00	2.08	1.93	1.95	1.99	2.07	1.93	2.03	2.01
glmax	0.0055	0.0055	0.0058	0.0061	0.0060	0.0049	0.0050	0.0055	0.0044	0.0049	0.0049
ths1	0.40	0.41	0.40	0.40	0.40	0.40	0.40	0.41	0.41	0.40	0.41
ths2	0.40	0.40	0.40	0.40	0.40	0.41	0.39	0.40	0.39	0.40	0.40
ths3	0.40	0.38	0.39	0.39	0.39	0.40	0.41	0.40	0.40	0.40	0.39
thr1	0.03	0.03	0.03	0.03	0.03	0.04	0.04	0.03	0.03	0.04	0.04
thr2	0.04	0.04	0.04	0.03	0.03	0.04	0.03	0.03	0.04	0.04	0.04
thr3	0.03	0.02	0.02	0.02	0.02	0.03	0.03	0.02	0.03	0.03	0.03
alpha1	4.61	4.30	4.88	4.57	4.73	4.78	4.41	4.38	4.59	4.93	4.40
alpha2	4.39	4.53	4.24	4.16	4.77	4.51	3.95	4.31	4.24	4.32	4.60
alpha3	4.16	4.46	4.21	4.58	4.25	4.33	4.54	4.51	4.42	4.31	4.58
npar1	2.27	2.01	2.32	2.24	2.19	2.09	2.03	1.76	1.73	1.65	2.04
npar2	1.53	1.70	2.09	1.83	2.13	1.60	1.75	1.84	1.76	2.15	2.01
npar3	2.18	2.30	2.33	2.37	2.33	2.29	1.99	2.33	2.23	2.29	2.41
ksat1	8070	7938	8002	8128	8089	8229	8216	7708	7578	7616	8113
ksat2	8219	7752	8042	7858	7912	7886	7725	7994	7936	7967	8348
ksat3	8132	8282	8421	8374	8308	8271	7867	8348	8286	8348	8504

Table S12 Determined parameter sets for Tharandt plot – mean of the 30 best simulation realted to KGE

	P 1	**P 2**	**P 3**	**P 4**	**P 5**	**P 6**	**P 7**	**P 8**	**P 9**	**P 10**	**P 11**
infexp	0.63	0.63	0.56	0.59	0.61	0.59	0.57	0.50	0.61	0.76	0.49
idepth	0.70	0.83	0.18	0.65	0.17	0.18	0.17	0.05	0.76	0.83	0.05
cvpd	1.98	2.05	2.06	2.05	2.07	1.99	1.93	2.12	2.02	2.01	2.08
glmax	0.0055	0.0053	0.0053	0.0054	0.0055	0.0053	0.0053	0.0053	0.0058	0.0048	0.0055
qffc	0.25	0.24	0.27	0.27	0.25	0.31	0.28	0.26	0.24	0.25	0.26
qfpar	0.28	0.25	0.19	0.27	0.19	0.20	0.16	0.25	0.30	0.28	0.27
ths1	0.47	0.48	0.46	0.50	0.46	0.45	0.45	0.48	0.46	0.47	0.48
ths2	0.47	0.48	0.48	0.45	0.47	0.48	0.47	0.47	0.47	0.48	0.47
ths3	0.48	0.48	0.46	0.48	0.46	0.46	0.47	0.48	0.49	0.47	0.48
thr1	0.06	0.08	0.09	0.10	0.08	0.10	0.09	0.10	0.06	0.06	0.10
thr2	0.05	0.08	0.06	0.05	0.07	0.05	0.08	0.07	0.05	0.07	0.06
thr3	0.09	0.06	0.05	0.08	0.05	0.06	0.05	0.05	0.08	0.12	0.05
alpha1	3.29	2.91	3.25	3.18	3.31	3.29	3.26	3.10	3.14	3.58	3.13
alpha2	3.39	3.00	3.20	3.42	3.08	3.06	3.28	3.45	3.49	3.34	3.57
alpha3	2.94	3.74	3.24	3.09	3.22	3.15	3.17	3.28	2.97	3.31	3.20
npar1	2.28	1.61	2.04	1.98	2.14	2.18	2.23	2.02	2.08	2.23	2.01
npar2	2.20	1.98	2.18	2.31	2.10	2.17	2.12	1.89	2.26	2.20	1.92
npar3	1.76	2.23	2.00	1.71	2.08	2.08	2.01	2.06	1.61	1.71	2.00
ksat1	840	634	780	598	809	858	866	709	683	704	657
ksat2	710	585	825	758	808	787	748	749	688	699	692
ksat3	729	591	693	589	749	673	708	753	734	752	701
gravel1	0.48	0.40	0.49	0.48	0.47	0.48	0.45	0.42	0.49	0.42	0.40
gravel2	0.41	0.39	0.50	0.39	0.50	0.53	0.49	0.47	0.41	0.44	0.46
gravel3	0.39	0.44	0.41	0.40	0.40	0.41	0.41	0.47	0.44	0.43	0.48

Table S13 Water balance for the years 2023 and 2024 at the Kienhorst site for the 11 Profiles, average of the 30 best calibrated simulations

		Prec. (mm)	Evap IC (mm)	Evap Soil (mm)	Srfl (mm)	Byfl (mm)	Dsfl (mm)	Tran (mm)	Vrfln (mm)	Vrfln (%)	Soil moisture storage (mm)
P1	**2023**	690	291	27	18	0	0	188	47	7	113
	2024	609	270	25	14	0	0	228	166	27	-94
P2	**2023**	690	291	32	18	0	0	172	57	8	113
	2024	609	270	34	15	0	0	209	175	29	-95
P3	**2023**	690	291	28	20	0	0	163	70	10	107
	2024	609	270	32	18	0	0	216	127	21	-89
P4	**2023**	690	291	28	19	0	0	171	60	9	114
	2024	609	270	29	15	0	0	214	165	27	-95
P5	**2023**	690	291	29	20	0	0	162	69	10	108
	2024	609	270	36	18	0	0	214	125	21	-89
P6	**2023**	690	291	30	18	0	0	176	56	8	112
	2024	609	270	31	14	0	0	214	173	28	-94
P7	**2023**	690	291	31	18	0	0	196	35	5	114
	2024	609	270	32	14	0	0	235	151	25	-94
P8	**2023**	690	291	35	19	0	0	171	55	8	113
	2024	609	270	40	15	0	0	209	159	26	-94
P9	**2023**	690	291	36	18	0	0	173	53	8	113
	2024	609	270	41	14	0	0	208	170	28	-94
P10	**2023**	690	291	35	19	0	0	164	61	9	113
	2024	609	270	42	16	0	0	203	159	26	-94
P11	**2023**	690	291	33	19	0	0	156	72	10	108
	2024	609	270	41	17	0	0	205	135	22	-90

Table S14 Water balance for the years 2023 and 2024 at the Tharandt site for the 11 profiles, average of the 30 best calibrated simulations

		Prec. (mm)	Evap IC (mm)	Evap Soil (mm)	Srfl (mm)	Byfl (mm)	Dsfl (mm)	Tran (mm)	Vrfln (mm)	Vrfln (%)	Soil moisture storage (mm)
P1	**2023**	864	308	50	0	125	0	238	106	12	39
	2024	745	255	43	0	106	0	247	114	15	-18
P2	**2023**	864	308	60	0	99	0	257	94	11	48
	2024	745	255	57	0	77	0	266	109	15	-17
P3	**2023**	864	308	68	0	300	0	176	6	1	8
	2024	745	255	56	0	254	0	182	7	1	-8
P4	**2023**	864	308	59	0	132	0	247	74	9	45
	2024	745	255	53	0	119	0	251	91	12	-22
P5	**2023**	864	308	67	0	309	0	172	8	1	2
	2024	745	255	54	0	264	0	173	3	0	-3
P6	**2023**	864	308	65	0	316	0	164	6	1	7
	2024	745	255	53	0	267	0	170	6	1	-6
P7	**2023**	864	308	65	0	325	0	156	7	1	4
	2024	745	255	54	0	279	0	157	4	1	-3
P8	**2023**	864	308	67	0	367	0	123	0	0	1
	2024	745	255	55	0	315	0	123	0	0	-2
P9	**2023**	864	308	53	0	92	0	260	99	12	52
	2024	745	255	47	0	78	0	271	118	16	-21
P10	**2023**	864	308	44	0	89	0	246	145	17	33
	2024	745	255	39	0	72	0	257	142	19	-17
P11	**2023**	864	308	67	0	362	0	127	0	0	1
	2024	745	255	55	0	310	0	127	0	0	-2

References

Andersson, J. C. M., Arheimer, B., Traoré, F., Gustafsson, D., and Ali, A.: Process refinements improve a hydrological model concept applied to the Niger River basin, Hydrol. Process., 31, 4540–4554, https://doi.org/10.1002/hyp.11376, 2017.

Bernhard, F., Seeger, S., Weiler, M., Gessler, A., and Meusburger, K.: Simulating soil-plant-atmosphere interactions for sub-daily in situ observations of stable isotopes in soil and xylem water to assess two-pore domain model hypothesis, Copernicus Meetings, https://doi.org/10.5194/egusphere-egu2020-17975, 2020.

Brutsaert, W.: Evaporation into the Atmosphere, Springer Netherlands, Dordrecht, https://doi.org/10.1007/978-94-017-1497-6, 1982.

Castaneda-Gonzalez, M., Poulin, A., Romero-Lopez, R., Arsenault, R., Brissette, F., Chaumont, D., and Paquin, D.: Impacts of Regional Climate Model Spatial Resolution on Summer Flood Simulation, HIC 2018. 13th International Conference on Hydroinformatics, 372–362, https://doi.org/10.29007/hd8l, 2018.

Davison, A. C. and Hinkley, D. V.: Bootstrap Methods and their Application, Cambridge University Press, Cambridge, https://doi.org/10.1017/CBO9780511802843, 1997.

Efron, B. and Tibshirani, R. J.: An Introduction to the Bootstrap, Chapman and Hall/CRC, New York, 456 pp., https://doi.org/10.1201/9780429246593, 1994.

Federer, C. A., Vörösmarty, C., and Fekete, B.: Sensitivity of Annual Evaporation to Soil and Root Properties in Two Models of Contrasting Complexity, 2003.

Fowler, J., Cohen, L., and Jarvis, P.: Practical Statistics for Field Biology, 2nd Edition | Wiley, 272 pp., 1998.

Gash, J. H. C.: An analytical model of rainfall interception by forests, Q. J. R. Meteorol. Soc., 105, 43–55, https://doi.org/10.1002/qj.49710544304, 1979.

van Genuchten, M. Th.: A Closed-form Equation for Predicting the Hydraulic Conductivity of Unsaturated Soils, Soil Sci. Soc. Am. J., 44, 892–898, https://doi.org/10.2136/sssaj1980.03615995004400050002x, 1980.

Gupta, H. V., Kling, H., Yilmaz, K. K., and Martinez, G. F.: Decomposition of the mean squared error and NSE performance criteria: Implications for improving hydrological modelling, J. Hydrol., 377, 80–91, https://doi.org/10.1016/j.jhydrol.2009.08.003, 2009.

Hazen, A.: Some physical properties of sands and gravels, with special reference to their use in filtration., Massachusetts State Board of Health, Massachusetts, 1892.

ICOS Ecosystem Station Kienhorst (DE-Kie): Integrated Carbon Observation System (ICOS) RI, Ecosystem Thematic Centre, 2025.

ICOS Ecosystem Station Tharandt (DE-Tha): Integrated Carbon Observation System (ICOS) RI, Ecosystem Thematic Centre, 2025.

Knoben, W. J. M., Freer, J. E., and Woods, R. A.: Technical note: Inherent benchmark or not? Comparing Nash–Sutcliffe and Kling–Gupta efficiency scores, Hydrol. Earth Syst. Sci., 23, 4323–4331, https://doi.org/10.5194/hess-23-4323-2019, 2019.

Koskinen, M., Tahvanainen, T., Sarkkola, S., Menberu, M. W., Laurén, A., Sallantaus, T., Marttila, H., Ronkanen, A.-K., Parviainen, M., Tolvanen, A., Koivusalo, H., and Nieminen, M.: Restoration of nutrient-rich forestry-drained peatlands poses a risk for high exports of dissolved organic carbon, nitrogen, and phosphorus, Sci. Total Environ., 586, 858–869, https://doi.org/10.1016/j.scitotenv.2017.02.065, 2017.

Manly, B. F. J. and Manly, B. F. J.: Randomization, Bootstrap and Monte Carlo Methods in Biology, 3rd ed., Chapman and Hall/CRC, New York, 480 pp., https://doi.org/10.1201/9781315273075, 2018.

Mualem, Y.: A new model for predicting the hydraulic conductivity of unsaturated porous media, Water Resour. Res., 12, 513–522, https://doi.org/10.1029/WR012i003p00513, 1976.

Richards, L. A.: CAPILLARY CONDUCTION OF LIQUIDS THROUGH POROUS MEDIUMS, Physics, 1, 318–333, https://doi.org/10.1063/1.1745010, 1931.

Rutter, A. J., Kershaw, K. A., Robins, P. C., and Morton, A. J.: A predictive model of rainfall interception in forests, 1. Derivation of the model from observations in a plantation of Corsican pine, Agric. Meteorol., 9, 367–384, https://doi.org/10.1016/0002-1571(71)90034-3, 1971.

Schönfelder, L. H., Bakken, T. H., Alfredsen, K., and Adera, A. G.: Application of HYPE in Norway, SINTEF Energy Research, 2017.

Shuttleworth, W. J. and Wallace, J. S.: Evaporation from sparse crops-an energy combination theory, Q. J. R. Meteorol. Soc., 111, 839–855, https://doi.org/10.1002/qj.49711146910, 1985.

Weis, W., Ahrends, B., Böhner, J., Falk, W., Fleck, S., Habel, R., Klemmt, H.-J., Meesenburg, H., Müller, A.-C., Puhlmann, H., Wehberg, J.-A., Wellpott, A., and Wolf, T.: Standortsfaktor Wasserhaushalt im Klimawandel, Zentrum Wald Forst Holz Weihenstephan, Freising, Freising, 2023.

Wösten, J. H. M., Lilly, A., Nemes, A., and Le Bas, C.: Development and use of a database of hydraulic properties of European soils, Geoderma, 90, 169–185, https://doi.org/10.1016/S0016-7061(98)00132-3, 1999.